NASA Technical Memorandum 84550

Image Degradation in Langley 0.3-Meter Transonic Cryogenic Tunnel

W. L. Snow, A. W. Burner,
and W. K. Goad

NOVEMBER 1982

NASA

NASA Technical Memorandum 84550

Image Degradation in Langley 0.3-Meter Transonic Cryogenic Tunnel

W. L. Snow, A. W. Burner,
and W. K. Goad
Langley Research Center
Hampton, Virginia

National Aeronautics
and Space Administration

**Scientific and Technical
Information Branch**

1982

INTRODUCTION

Cryogenic wind tunnels are being developed to enable aerodynamic testing at realistic Reynolds numbers. Such facilities take advantage of the increasing density and viscosity associated with cooling so that when operating at high pressures, these tunnels can simulate full-scale Reynolds numbers. Under the high dynamic pressures available in many of these test environments, large and slender models can deform considerably. Wing tips may deflect 5 to 8 cm (2 to 3 in.) over 76-cm (30-in.) spans for some configurations in these cryogenic wind tunnels. Unless this wing deflection (model deformation) can be measured, the aerodynamicist is faced with the dilemma of having unique data on an unknown model geometry. At the National Transonic Facility (NTF) that is under construction at Langley, virtually all the proposed techniques being considered to discern model deformation, which include stereo photogrammetry, moiré topology, and surface light emitting diode (LED) trackers, presume that identifiable targets can be viewed clearly and unambiguously through the flow field. The purpose of this study was to gain experience with imaging through a cryogenic flow field. It is anticipated that such experience will aid in the design and operation of a proposed model-deformation-measuring system for the NTF.

DESCRIPTION OF THE TEST CONFIGURATION

The Langley 0.3-Meter Transonic Cryogenic Tunnel (0.3-m TCT) is a continuous-flow, fan-driven tunnel, which uses nitrogen as a test gas and is cooled by injecting liquid nitrogen directly into the stream. Varying the rate of liquid nitrogen injection provides a total temperature T_t range from 80 to 330 K while the total pressure p_t can be varied from 1.2 to 6.0 atm (1 atm = 101.325 kPa). The combined low temperature and high pressure can produce a Reynolds number of over 330×10^6 per meter. Some of the design features and operational characteristics of the 0.3-m TCT have been reported by Kilgore in reference 1. A schematic of the 0.3-m TCT circuit is shown in figure 1.

Viewing models in a transonic wind tunnel is complicated, since the primary flow duct is surrounded by a plenum into which some of the flow is vented through slots or porous walls. For cryogenic tunnels, viewing ports in the pressure shell, which must be provided for optical access to the flow field, are typically purged with dry room-temperature nitrogen to prevent moisture condensation and eventual frost buildup as the outer optical surfaces reach the freezing temperature of water.

The 0.3-m TCT accommodates a two-dimensional test-section insert as shown in figure 2. For this study and other flow visualization tests, the Plexiglas windows labeled "view ports" in figure 2 were replaced with schlieren quality fused silica D-shaped windows. The model used in this study, an airfoil, is below the lower edge of the D-shaped windows and is not visible through the viewing port as depicted in figure 3. A top view of the test section is seen in figure 4, which shows the slotted floor. However, these photographs do not show the 23-cm (9-in.) diameter windows in the pressure shell which are centered on the turntable axis. When the larger windows are in place, equipment pods (fig. 5) designed to contain schlieren optics are attached to each side. Originally, these pods served as safety buffers against window rupture during high pressure runs. The pods are also used as test stands for optical experiments involving the flow field.

The 70-mm format camera used in the study was equipped with a telephoto lens augmented with a close-up adapter to shorten its near focus. The camera was mounted in the equipment pod on a traversing screw (see fig. 6) having 40 threads per inch. The position was monitored with a shaft encoder with remote digital readout. One count corresponded to one shaft revolution. The locations for best focus were noted by visual inspection and verified by subsequent photographs. The camera could be positioned during the run by using the digital readout.

The experimental setup for viewing the airfoil through the side windows is depicted in figure 6. Optical targets were placed on each of the four windows (stations 1 to 4). The camera was remotely tracked to focus separately on each target in order to assess cumulative image degradation caused by additional path lengths through the test gas.

When the top of the airfoil is to be viewed, illumination is provided through the D-shaped windows. A lens relay system is required to transfer the image of the airfoil through a viewing port located at the top of the test section where it can be photographed and/or viewed with a television camera. Figure 7 shows a schematic of the experimental setup. The ground glass screen of the film camera used for reflex viewing was replaced with a field lens to provide full field coverage for a closed circuit television (CCTV). The CCTV was used to monitor the airfoil in the control room during the tunnel runs.

MODEL DEFORMATION CONSIDERATIONS

A sufficient number of clearly identifiable reference points (or optical targets) are placed on the model surface so that tracking their location adequately describes model deformation. Pairs of photographs of the targets can be used to track their three-dimensional location and hence the model surface topology. Yet to be resolved is the problem of providing high contrast reference points on a shiny surface while holding surface tolerance to a fraction of a micrometer (ref. 2) to avoid drag penalties or flow perturbations. Thermal stresses further complicate the problem and preclude the use of "drill and fill" approaches for cryogenic models.

The reference points are viewed through dense flow fields with expected discontinuities in the form of shocks. Turbulence within the flow and especially at boundary layers is expected to degrade the imagery. Figure 8, from reference 3, shows an example of boundary effects on focused shadow photographs. To ascertain how well the flow field behaves as an optical element, the concept of modulation transfer is invoked.

MODULATION TRANSFER FUNCTION

The flow field can be treated as any other optical component and in particular can be indexed by its modulation transfer function (MTF) to quantify its imaging qualities. The utility of this concept is well established for optical design purposes, and only the rudiments of this elegant approach are given here (ref. 4, chapter 11, and ref. 5).

The information in a scene can be decomposed into its spatial frequency components. Linear systems can alter the phase and amplitude of these components while leaving the frequency invariant. Resynthesis of the modified components reconstructs the degraded image of the scene. A sinusoidal target is photographed and its trans-

mittance T (the optical density $D \equiv -\log_{10} T$) is measured with a microdensitometer. From the relative calibration of the film, known as the Hurter and Driffield (H & D) curve, these values of transmittance can be translated to relative exposure levels E at the film plane. Then, the modulation M is defined as

$$M = \frac{E_{max} - E_{min}}{E_{max} + E_{min}} \tag{1a}$$

If the scene is now viewed through a less than ideal medium and the procedure repeated to yield

$$M' = \frac{E'_{max} - E'_{min}}{E'_{max} + E'_{min}} \tag{1b}$$

then the modulation transfer function (MTF) is

$$MTF = \frac{M'}{M} \tag{2}$$

An ideal medium (vacuum) would have a unit transfer function extending to all frequencies. In practice, the MTF rolls off severely at higher frequencies.

EXPECTED FLOW FIELD EFFECTS

Image degradation caused by the dense cryogenic flow field can be broadly classified into static and dynamic categories. The dynamic category would include flow-related effects such as shock-related density discontinuities, perturbations from turbulent boundary layers over model and viewing port surfaces, scattering from condensation, and blurring due to vibration. Static effects would include focus shifts due to increased optical depth related to gas density, relative component motion due to thermal expansion, density fluctuations due to thermal gradients, and condensation on windows.

To fully utilize the benefits of increased density, the cryogenic facility must operate as close as possible to the liquid-vapor condensation line. The Clausius-Clapeyron equation is given by

$$\log_{10} p = -\frac{A}{T} + B \tag{3}$$

where the empirical constants A and B for nitrogen are, respectively, 314.22 K and 4.0679 atm (ref. 6, p. 311) and T is in kelvins and p is in atmospheres.

This equation represents the locus of static conditions which must prevail in the flow for condensation to occur. The total pressure p_t and total temperature T_t which would lead to these conditions may be obtained by using the following well-known relations:

$$\frac{T}{T_t} = \left(1 + \frac{\gamma - 1}{2} M^2\right)^{-1} = \left(1 + \frac{M^2}{5}\right)^{-1} \tag{4}$$

$$\frac{p}{p_t} = \left(1 + \frac{\gamma - 1}{2} M^2\right)^{-\gamma/(\gamma-1)} = \left(1 + \frac{M^2}{5}\right)^{-7/2} \tag{5}$$

where M is Mach number and the ratio of specific heats γ has been assumed to equal 1.4. Substituting equations (4) and (5) into equation (3) results in the following expression in terms of the total conditions, which are controlled by tunnel operators:

$$\left.\begin{aligned} \log_{10} p_t &= -\frac{A}{T_t}\left(1 + \frac{\gamma - 1}{2} M^2\right) + \left(\frac{\gamma}{\gamma - 1}\right)\log_{10}\left(1 + \frac{\gamma - 1}{2} M^2\right) + B \\ &= -\frac{A}{T_t}\left(1 + \frac{M^2}{5}\right) + \frac{7}{2}\log_{10}\left(1 + \frac{M^2}{5}\right) + B \end{aligned}\right\} \tag{6}$$

with $\gamma = 1.4$ again assumed. A family of plots of p_t versus T_t can be generated for free-stream and maximum local Mach numbers (M_∞ and $M_{\ell,max}$) for a particular test configuration, with the maximum local Mach number being dependent on the airfoil and its orientation. Typical p_t vs T_t curves are shown in figure 9. Visibility in the test section is drastically reduced at conditions near the phase transition line. The fictitious locus of conditions labeled (a) through (d) in figure 9 are typical of what might produce the indexed photographs in figure 10. Conditions (a), located well into the vapor region, produce high visibility. Conditions (b) and (c) are located in the region of local saturation over the airfoil, while conditions (d) are in the region of free-stream saturation, resulting in complete "white out." Previous work has demonstrated that the onset of condensation can be reasonably predetermined and therefore judiciously avoided (refs. 7 and 8).

Focus shifts due to thermal expansion are so configuration dependent that results obtained in one facility are not easily translated to another. To avoid window condensation, the viewing ports are purged with dry nitrogen between exposures. The effects of thermal gradients are difficult to assess since the camera is in an environment close to ambient while the test section is at cryogenic temperatures. In the NTF such problems might be lessened because the cameras will be located in the plenum in temperature- and pressure-controlled housings.

To measure the effect of the tunnel flow on the optical system response, a series of square wave optical targets at various spatial frequencies was attached to the model and the MTF was obtained for the flow field at various conditions. The modulation function of the square wave is always higher than that of the corresponding sine wave (ref. 9) because of contributions from odd harmonics. For more precise testing, corrections to the square wave results are included to recover the sine wave response. But for this work, the square wave response was used directly and thus gives a conservative estimate of the sine wave response. The square wave response is essentially the MTF as defined in equation (2). Standard sensitometry techniques were used to measure the response as described in chapter 14 of reference 9. A step tablet was registered on each film with a flash sensitometer. The specular density of the step filter and its processed image on the data record were measured with a recording microdensitometer to provide an H & D curve relating optical density to relative exposure. Tracings of Sayce targets were translated into relative intensities and the modulation determined from equation (1). Finally the square wave response was determined (eq. (2)).

TARGET PREPARATION CONSIDERATIONS

Several types of optical targets were tried in these tests. In some cases, machinist's dyes were stenciled on the surface and/or rub-on decals were applied. The decals less than 0.00254 cm (0.001 in.) thick, were usually overcoated with a clear lacquer to help adhere them to the shiny surface.

Shown in figure 11 are two photographs taken of a TV monitor using the apparatus shown in figure 7. The top photograph (fig. 11(a)) shows a series of 1.3-mm-diameter dots on the wing surface as they appear prior to test. The lower photograph (fig. 11(b)) shows a different scheme including several dye patterns. This photograph was taken during a run and some of the decal pattern had blown away. The tunnel conditions were close to the onset of condensation, and the slight contrails emanating from the edges of the targets emphasize the need for extreme care not to alter the model surface. More reliable techniques for applying optical targets to models will be required for the model deformation tests in the NTF.

To obtain the spatial frequency data for calculation of the flow field MTF, a Sayce target was used. (See the insert in fig. 6.) This target is available commercially on 10 × 20 × 0.64 cm (4 × 8 × 1/4 in.) high resolution plate and covers a spatial frequency range of 0.25 to 5 lines per millimeter. In the first series of tests, the flow field was observed through the side viewing ports of the tunnel and the Sayce target was used directly since it was outside the flow at station 4 in figure 6. For the second series of tests, the airfoil surface was observed from the top viewing ports of the tunnel. For these tests from the top the Sayce target was contact printed onto stripping film that could then be glued to the airfoil surface. The thickness of the stripping film emulsion and glue was less than 25 μm. The targets can be seen in figure 10 and in larger format in figure 12. Sayce targets were placed along and transverse to the flow. Measurements were made along the chord since no obvious transverse gradients were noted. Ink dots and a stenciled pattern with marks at 10 percent chord stations were added for condensation studies similar to those described in reference 7. To differentiate between the optical response of the flow in the test section and the plenum, targets were affixed to the windows at the four stations in figure 6 for a third series of tests. Figure 13 shows how these strips were located so that the camera could look "over the top" of consecutive targets.

RESULTS

Results of the side view tests are shown in figure 14. Two conditions are included. The mildest condition tested was 250 K at 1.2 atm represented by figures 14(a) and 14(b) and the most severe test was at 120 K and 5.0 atm shown in figures 14(c) and 14(d). The tests with the fan off were planned initially to study the effects of removing the turbulent boundary layers. Fortunately this test also made a troublesome vibration problem apparent as can be seen by comparing trace (1) in figures 14(c) and 14(d). Since station 1 was entirely outside of the test gas, image degradation at this station was attributed to vibration. There is a conspicuous increase of noise and vibration in the adjacent control room when the tunnel operates near the high pressure limit. The spread in figure 14(a) is probably typical of scatter in the data when modulation is high.

Barring vibration, the flow field at the milder conditions produced little or no image degradation. Figure 14(c), however, shows that at higher densities the test-section gas introduces considerable deterioration. The plenum chambers, though contributing greater optical depth (see table I), do not significantly add to response degradation.

Results of the top view tests were comparable to side view results. The response functions would fall in the vicinity of trace (3) in figures 14(a) and 14(c). These data appeared to be less sensitive to vibration. The path length in the test section was slightly larger than that for station 3, but the plenum path was much reduced because of the facility design.

IMPLICATIONS FOR TARGET DISCRIMINATION

The consequences of decreasing square wave response for photogrammetric applications can be seen from the following discussion. An ideal target would be characterized by high contrast and sharp edges. A densitometer trace of the target image would approximate a rectangular pulse. The Fourier decomposition of such a pattern can be written as

$$f(x) = A\frac{d}{X} + 2A\frac{d}{X}\sum_{n=1}^{\infty} C_n \cos n2\pi f_o x \tag{7}$$

where $f_o \equiv 1/X$ and $C_n = (\sin n\pi f_o d)/n\pi f_o d$. Note that C_n is the transform of a rectangular pulse of amplitude A sampled at discrete frequencies $f \equiv f_n = nf_o$, which are multiples of the fundamental f_o. The discrete sampling imposes the periodicity. As X increases, the amplitude spectrum decreases and the continuous function $(\sin 2\pi fd)/\pi fd$ is sampled more frequently. Figure 15 depicts the positive half of an ideal target of dimension d centered on the origin. From figure 14(c), the square wave response drops off in an approximately linear fashion from unity at 0 frequency to zero at 3 lines per millimeter in the object plane at 120 K and 5 atm. If each of the coefficients in equation (7) is attenuated by the appropriate amount due to this response and the truncated series reevaluated, the result is as shown in figure 15 by the curve labeled "120 K/5 atm." The test-section gas at 5 atm and 120 K results in a redistribution of energy and a reduction in edge sharpness. To

conserve energy, the peak amplitude must decrease as shown, and an observer attempting to locate such a target under the reticle of a comparator would note its lower contrast. This amount of degradation would not significantly impact the accuracy of a photogrammetric application. The cutoff frequency should not be misconstrued to mean that details smaller than its reciprocal would completely vanish. Considerable information is carried in the first several harmonics, so that an object may be detected even if the detail dependent on higher frequency is lost.

CONCLUSION

The flow field of a cryogenic wind tunnel has been treated as an optical component indexed by its modulation transfer function. Tests were performed under conditions which avoided condensation. Under normal flow conditions, image degradation caused by boundary layer effects were masked by vibrational degradation. With the fan off, both of these degradations were removed, but the square wave response was still significantly lower at high spatial frequencies, especially at the high pressure and low temperature conditions (15 times atmospheric density). Furthermore, the degradation seemed to be localized in the test section and not the plenum. The reasons for this have not been determined. The degradation of imagery does not appear to be severe from a photogrammetry standpoint.

Langley Research Center
National Aeronautics and Space Administration
Hampton, VA 23665
October 20, 1982

REFERENCES

1. Kilgore, Robert A.: Design Features and Operational Characteristics of the Langley 0.3-Meter Transonic Cryogenic Tunnel. NASA TN D-8304, 1976.

2. Teague, E. Clayton; Vorburger, Theodore V.; Scire, Fredric E.; Baker, Saul M.; Jensen, Stephen W.; Trahan, Clare; and Gloss, Blair B.: Evaluation of Methods for Characterizing Surface Topography of Models for High Reynolds Number Wind-Tunnels. AIAA-82-0603, Mar. 1982.

3. Stine, Howard A.; and Winovich, Warren: Light Diffusion Through High-Speed Turbulent Boundary Layers. NACA RM A56B21, 1956.

4. Smith, Warren J.: Modern Optical Engineering. McGraw-Hill Book Co., Inc., c.1966.

5. Scott, Roderic M.: The Practical Application of Modulation Transfer Functions. Phot. Sci., Eng., vol. 9, no. 4, July-Aug. 1965, pp. 235-264.

6. Wegener, P. P.; and Mack, L. M.: Condensation in Supersonic and Hypersonic Wind Tunnels. Advances in Applied Mechanics, Volume V, H. L. Dryden and Th. von Kármán, eds., Academic Press Inc., 1958, pp. 307-447.

7. Hall, Robert M.: Onset of Condensation Effects With an NACA 0012-64 Airfoil Tested in the Langley 0.3-Meter Transonic Cryogenic Tunnel. NASA TP-1385, 1979.

8. Hall, Robert M.; Dotson, Edward H.; and Vennemann, Dietrich H.: Homogeneous and Heterogeneous Condensation of Nitrogen in Transonic Flow. NASA paper presented at 13th International Symposium on Rarefied Gas Dynamics (Novosibirsk, USSR), July 1982.

9. Thomas, Woodlief, Jr., ed.: SPSE Handbook of Photographic Science and Engineering. John Wiley & Sons, Inc., c.1973.

TABLE I.- PATH LENGTH FROM CAMERA TO SAYCE TARGETS AFFIXED TO TUNNEL WINDOWS

Region of tunnel	Path length, in., at station[a] -			
	1	2	3	4
Equipment pod	40	35	27	22
Plenum	0	5	5	10
Test section	0	0	8	8
Total	40	40	40	40

[a]See figure 6.

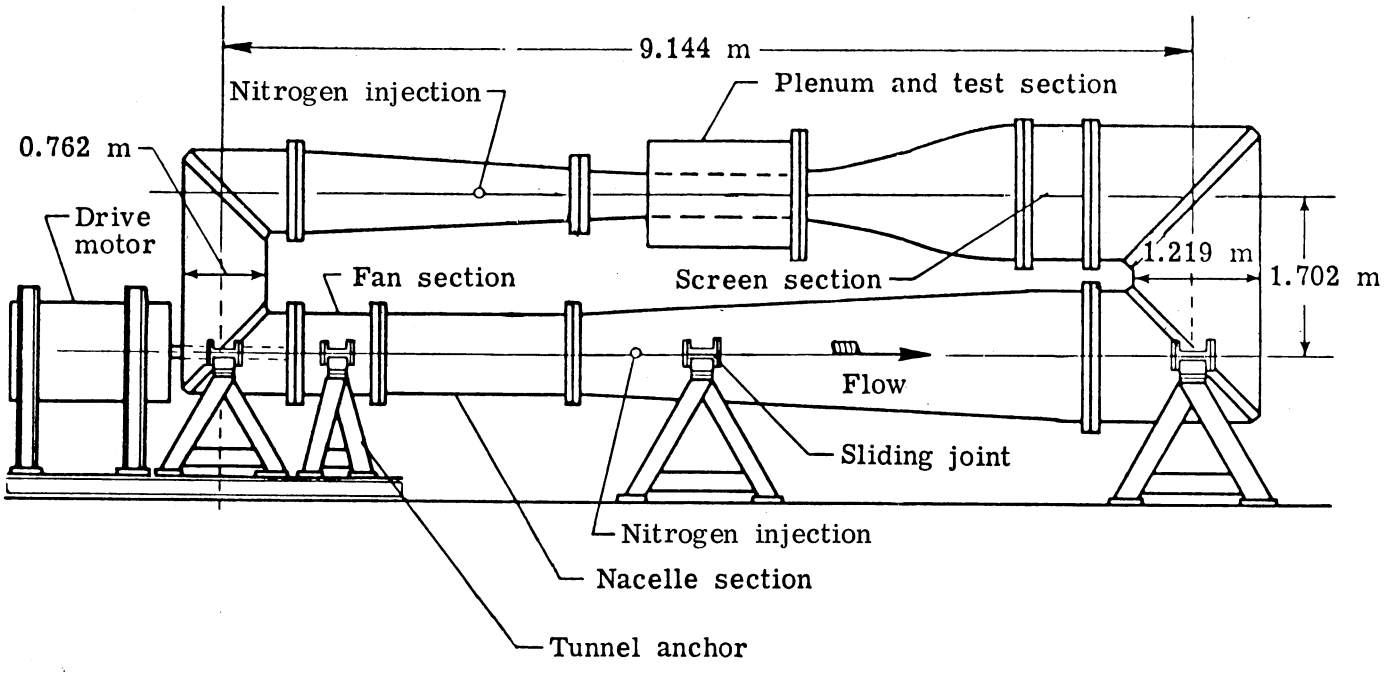

Figure 1.- Schematic of Langley 0.3-Meter Transonic Cryogenic Tunnel.

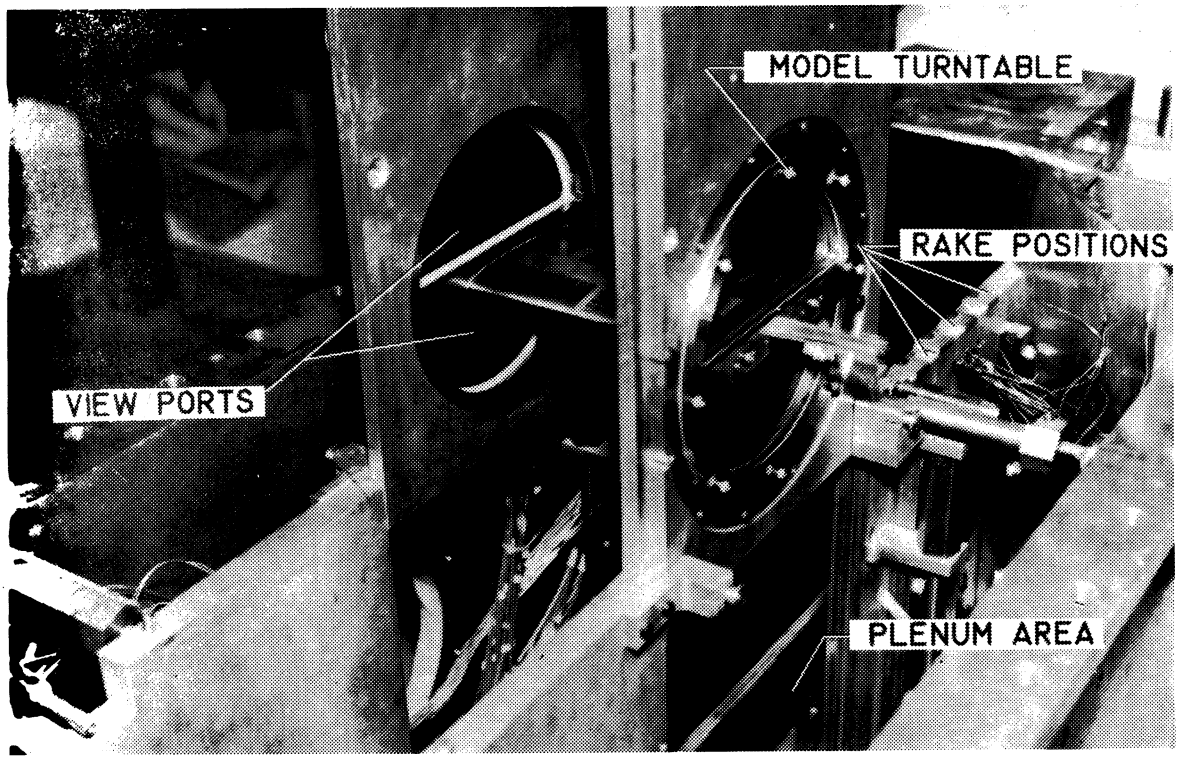

Figure 2.- Test-section view showing model turntable.

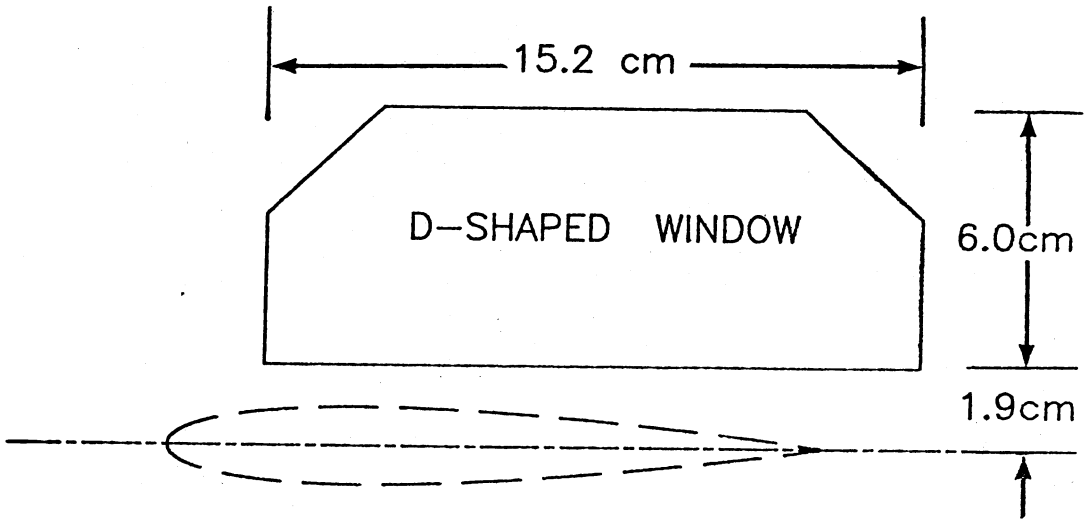

Figure 3.- Relationship between viewing port and airfoil.

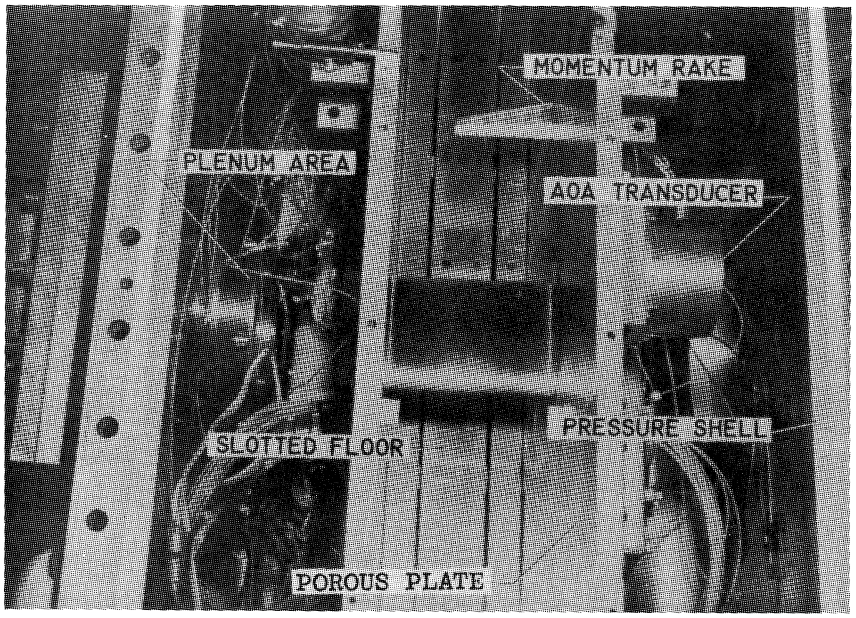

Figure 4.- Top view of test section with lid removed.

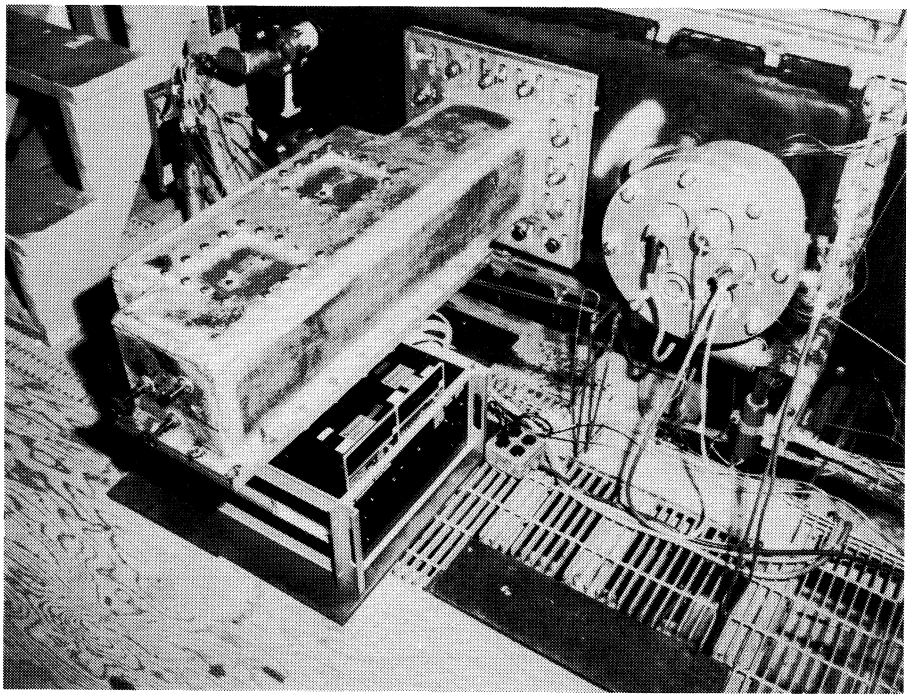

L-82-187

Figure 5.- Equipment pod designed for schlieren optics.

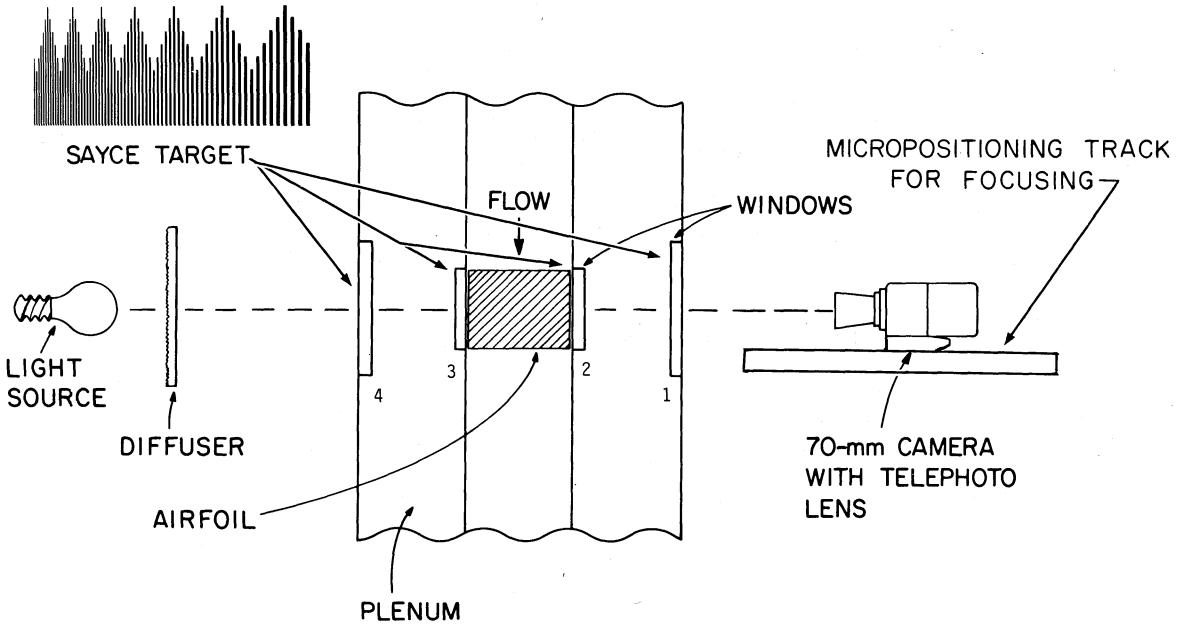

Figure 6.- Schematic of apparatus used for cross-flow photographs.

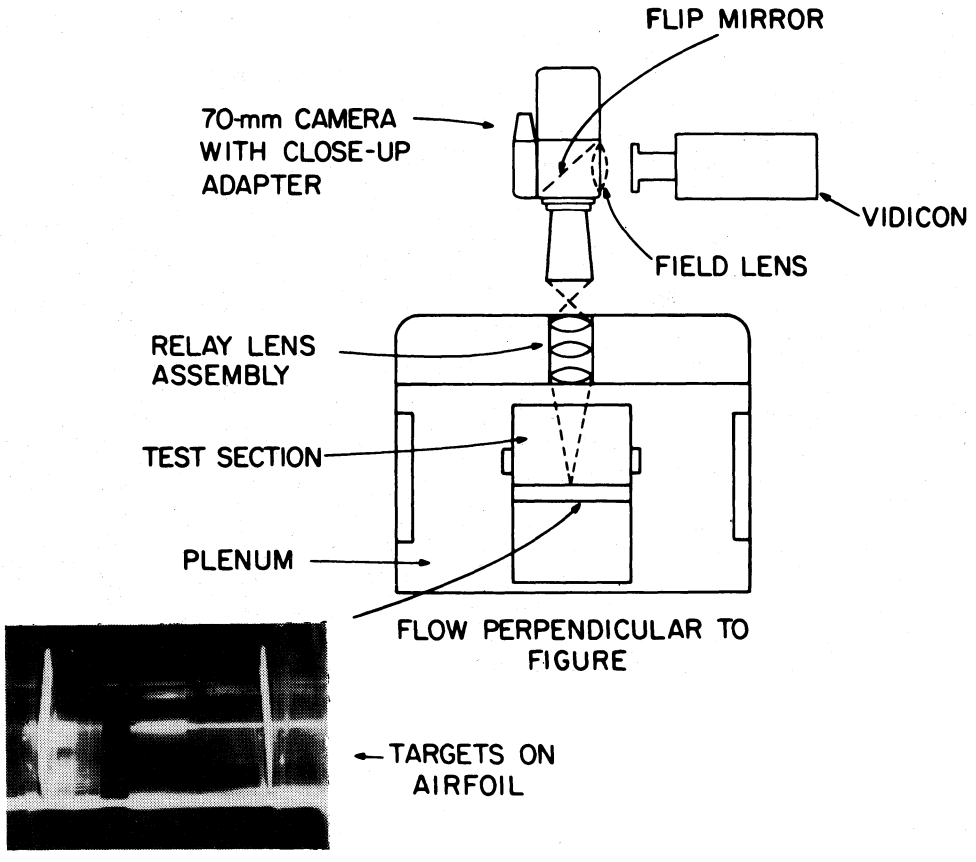

Figure 7.- Schematic of apparatus used to photograph top of airfoil.

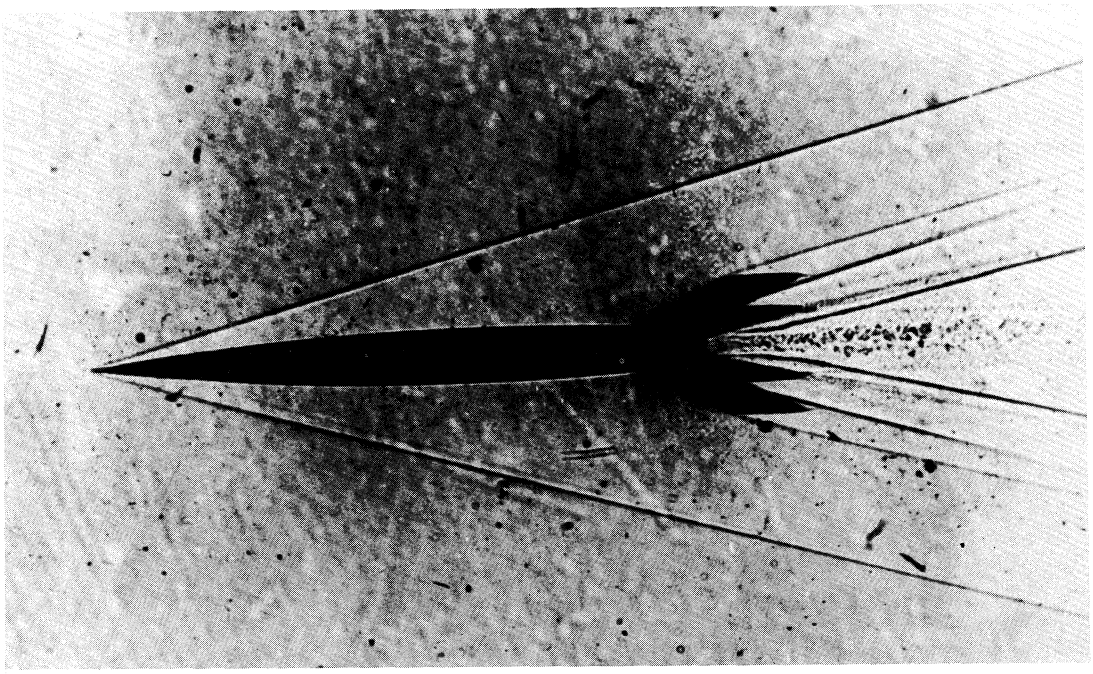

(a) Missile fired through quiescent air.

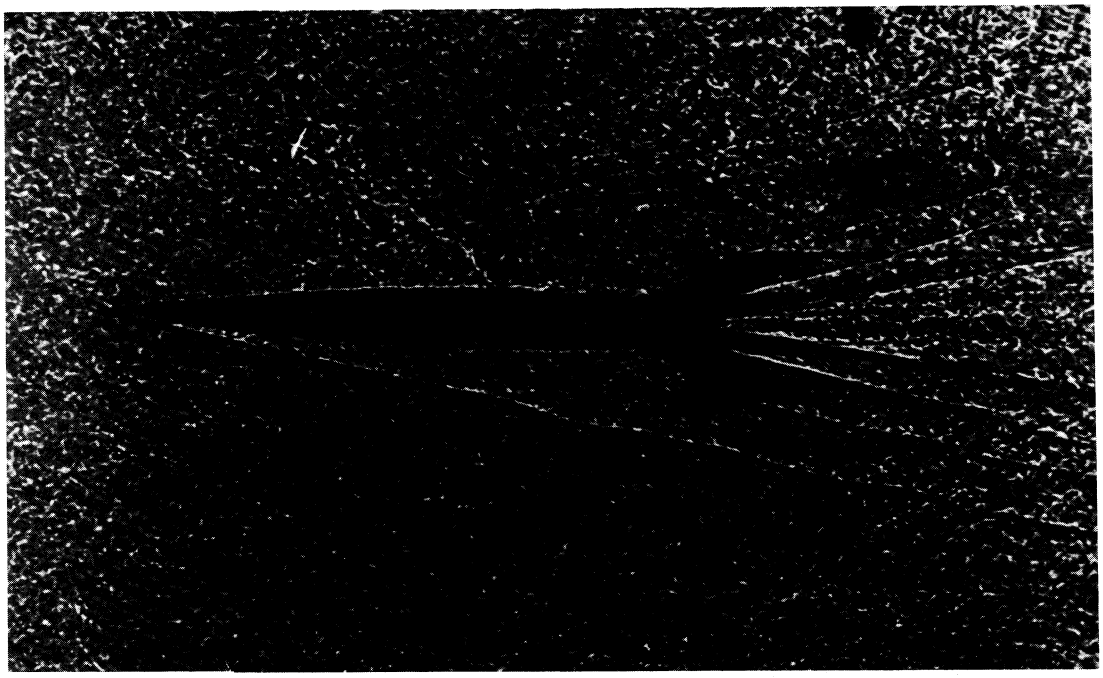

(b) Missile fired into counter flow at Mach 2.0.

Figure 8.-Shadow photographs of missile models in Ames supersonic free-flight wind tunnel showing the effect of turbulent sidewall boundary layers on a collimated light beam. Photo from reference 3.

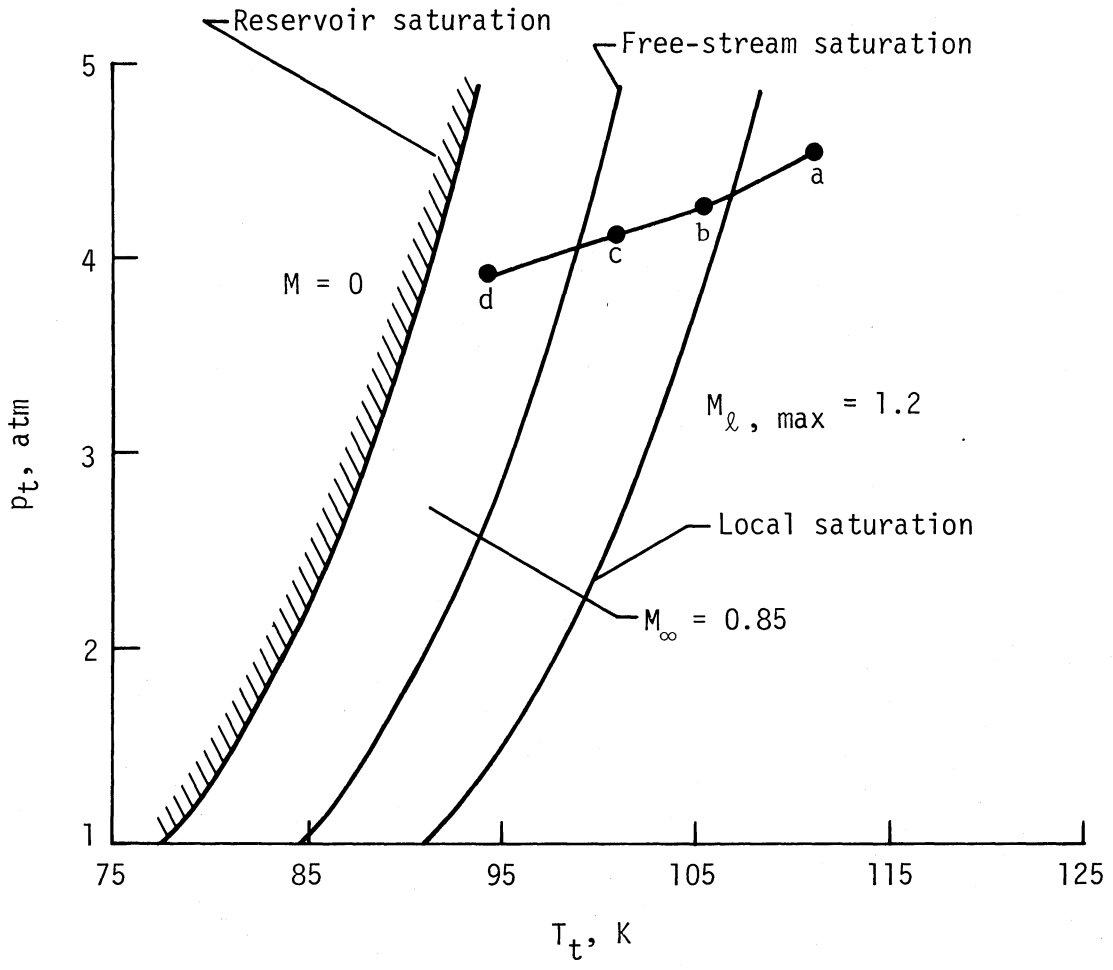

Figure 9.- Illustrative graph to indicate potential condensation regimes (ref. 6).

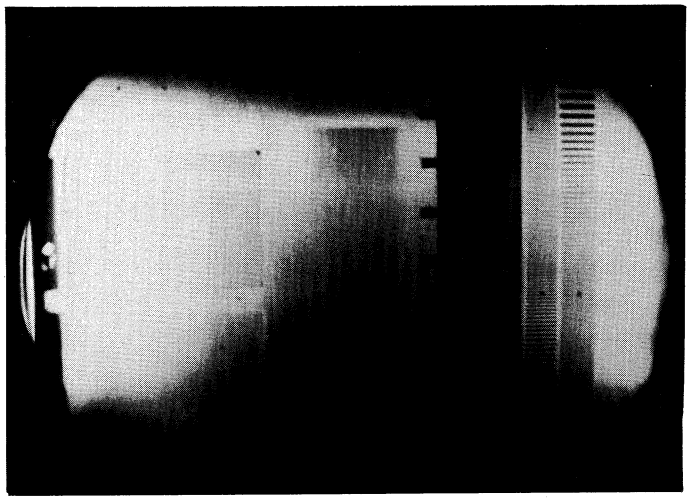

(a) Conditions (a) well away from saturation (point (a) in fig. 9).

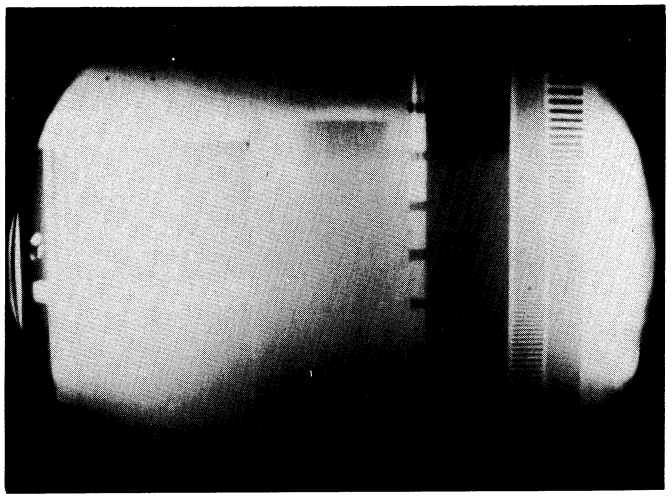

(b) Conditions (b) for which local saturation is possible (point (b) in fig. 9).

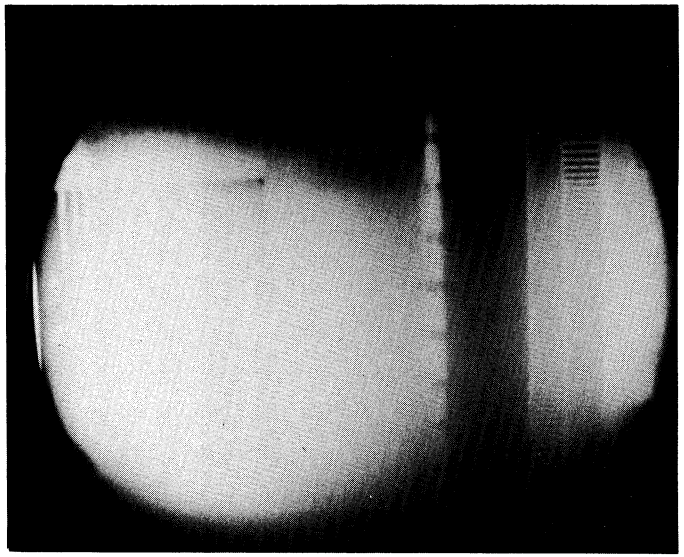

(c) Conditions (c) closer to free-stream saturation (point (c) in fig. 9).

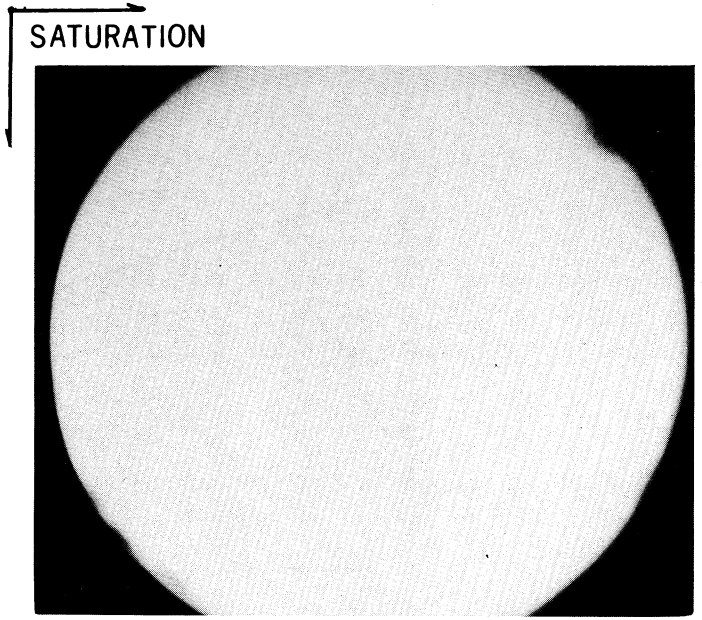

(d) Conditions (d) well within free-stream saturation (point (d) in fig. 9).

L-82-188

Figure 10.- Plan views of airfoil as condensation line is approached. (See fig. 9).

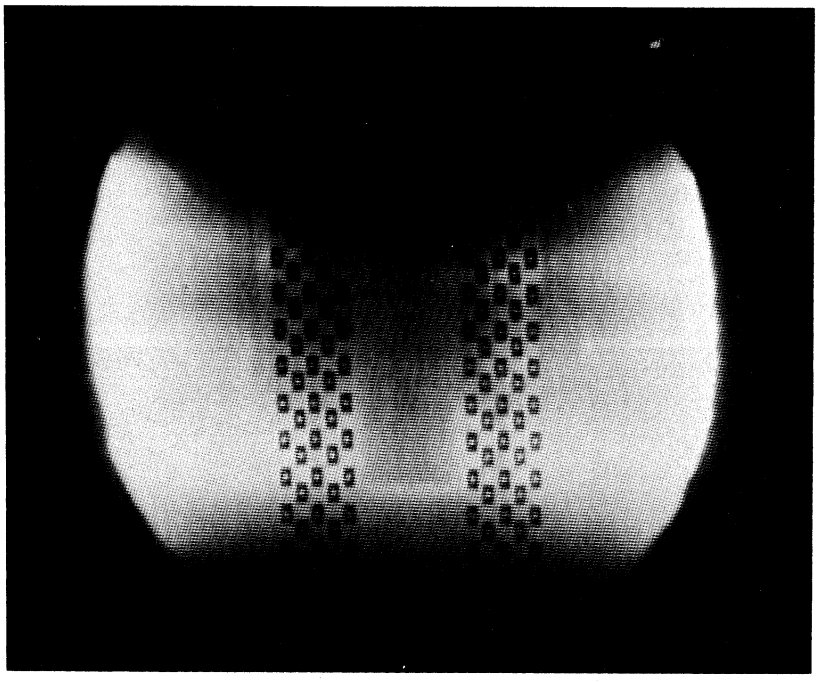

(a) Transfer decals are shown before run with 1.3-mm-diameter dots arranged chordwise on airfoil.

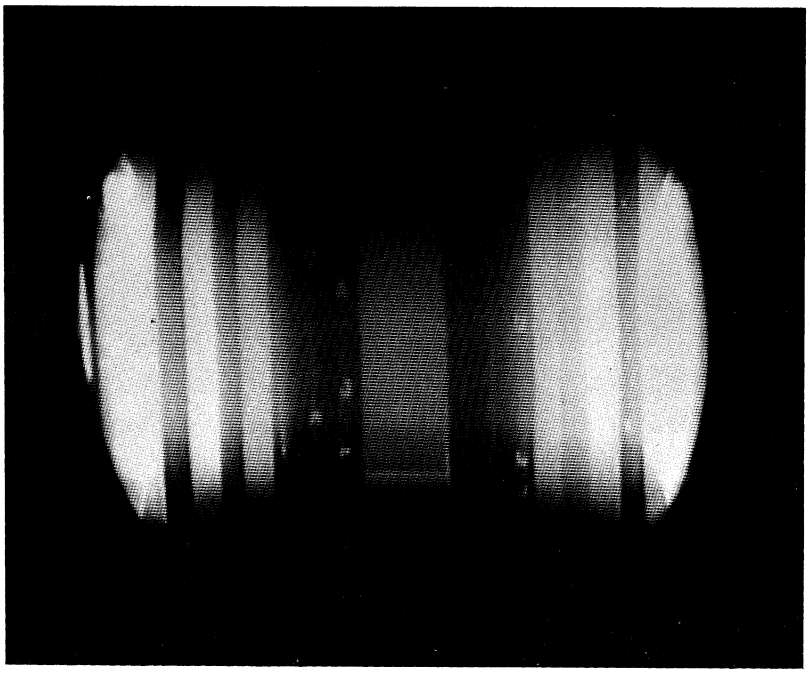

(b) Dye patterns with decals included in center pair; most decals were blown away during run.

L-82-189

Figure 11.- Two target approaches.

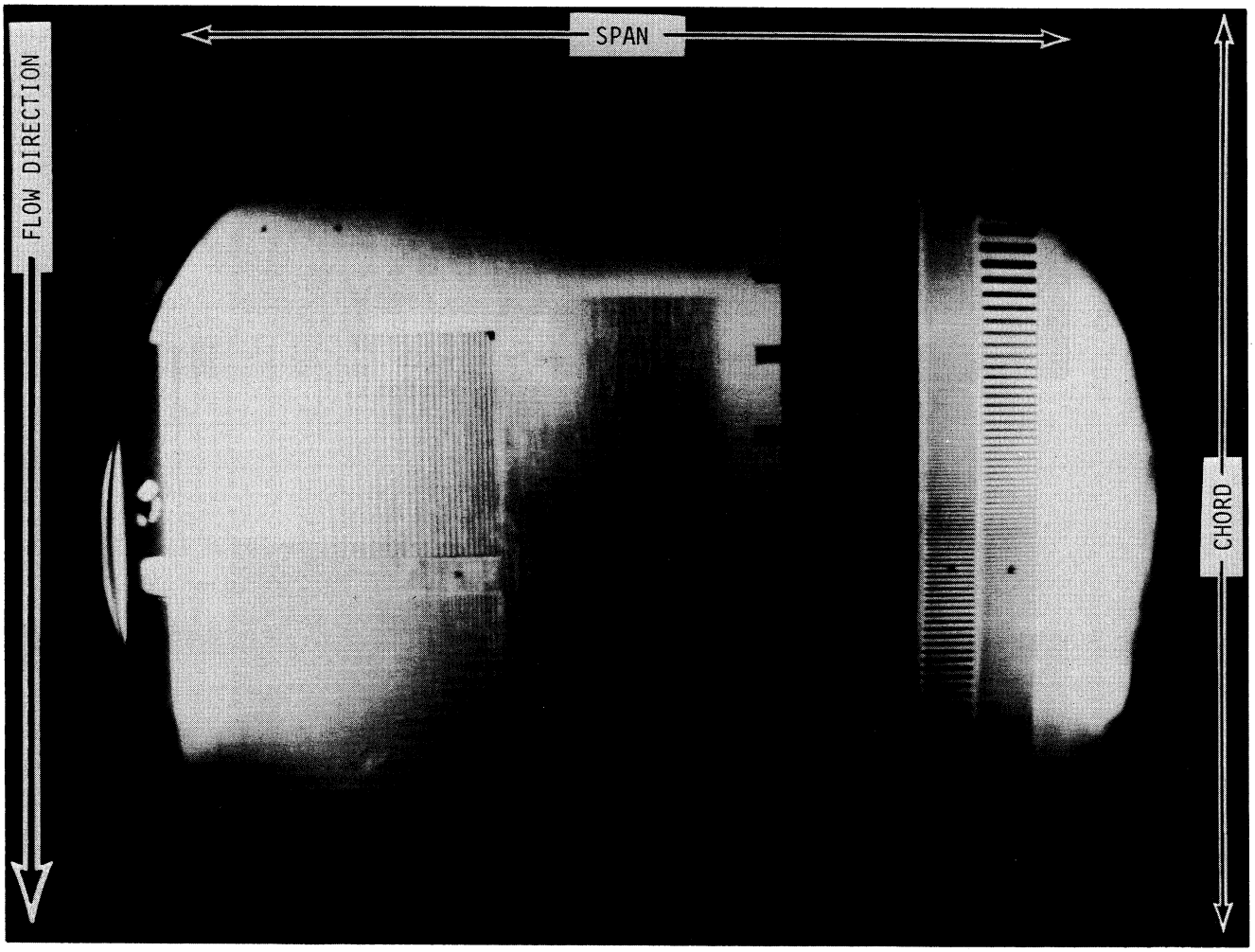

L-82-190

Figure 12.- Enlarged top view to indicate placement of Sayce targets in relation to flow.

Station 1

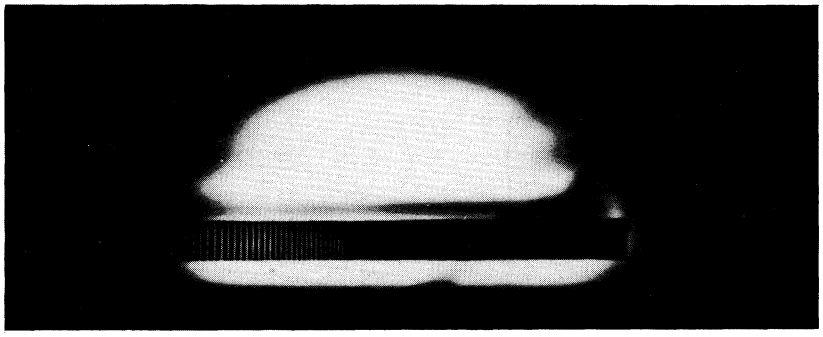

Station 2

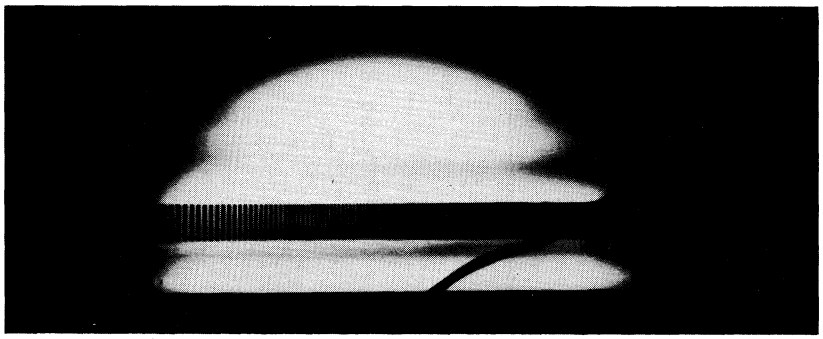

Station 3

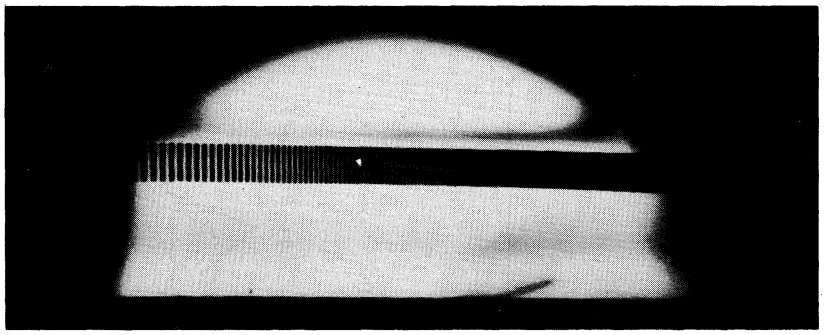

Station 4

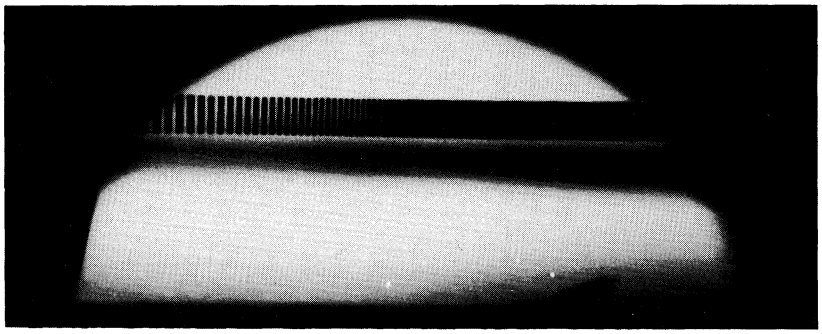

L-82-191

Figure 13.- Four station targets using apparatus of figure 6.

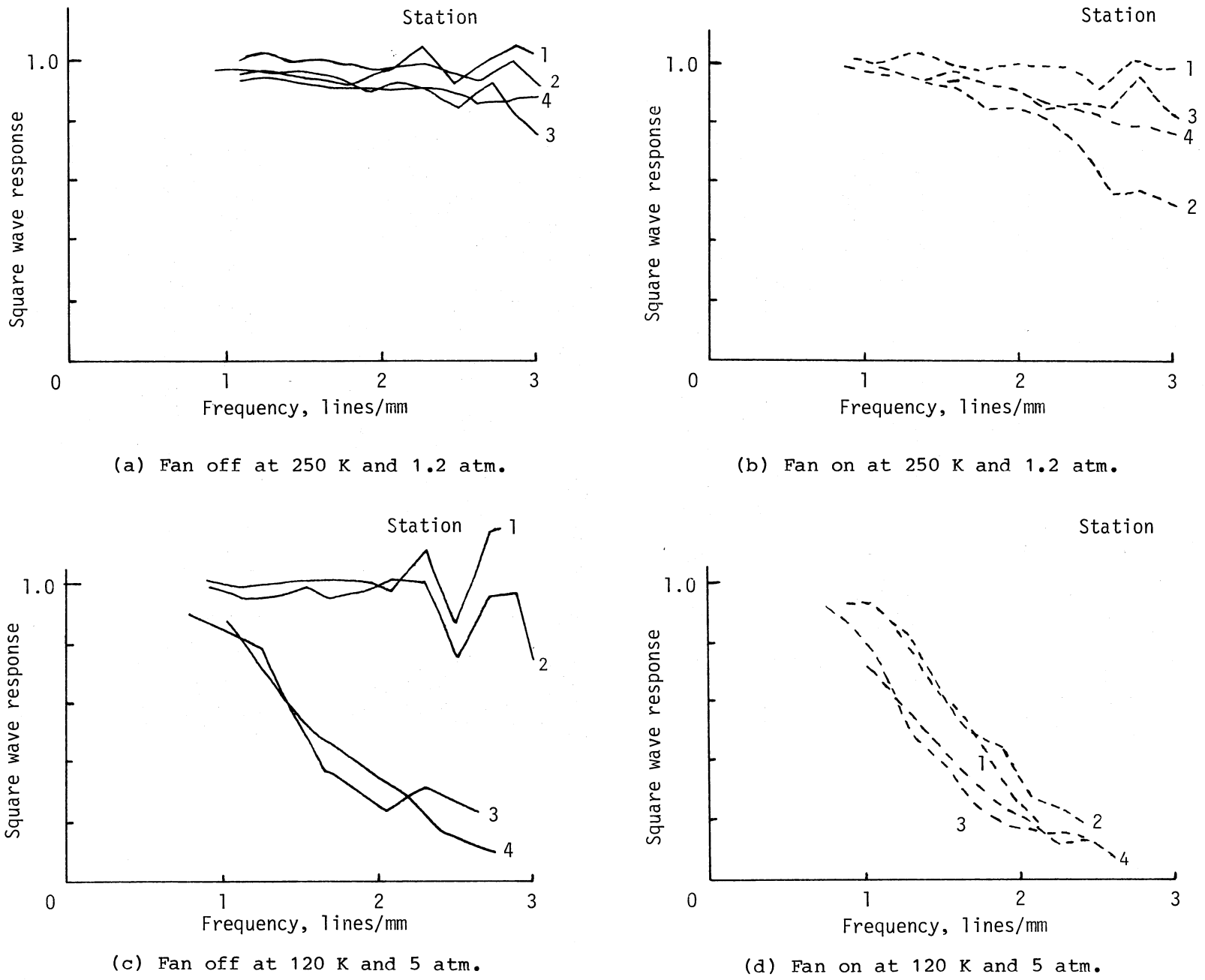

(a) Fan off at 250 K and 1.2 atm.

(b) Fan on at 250 K and 1.2 atm.

(c) Fan off at 120 K and 5 atm.

(d) Fan on at 120 K and 5 atm.

Figure 14.- Square wave response from cross-flow tests.

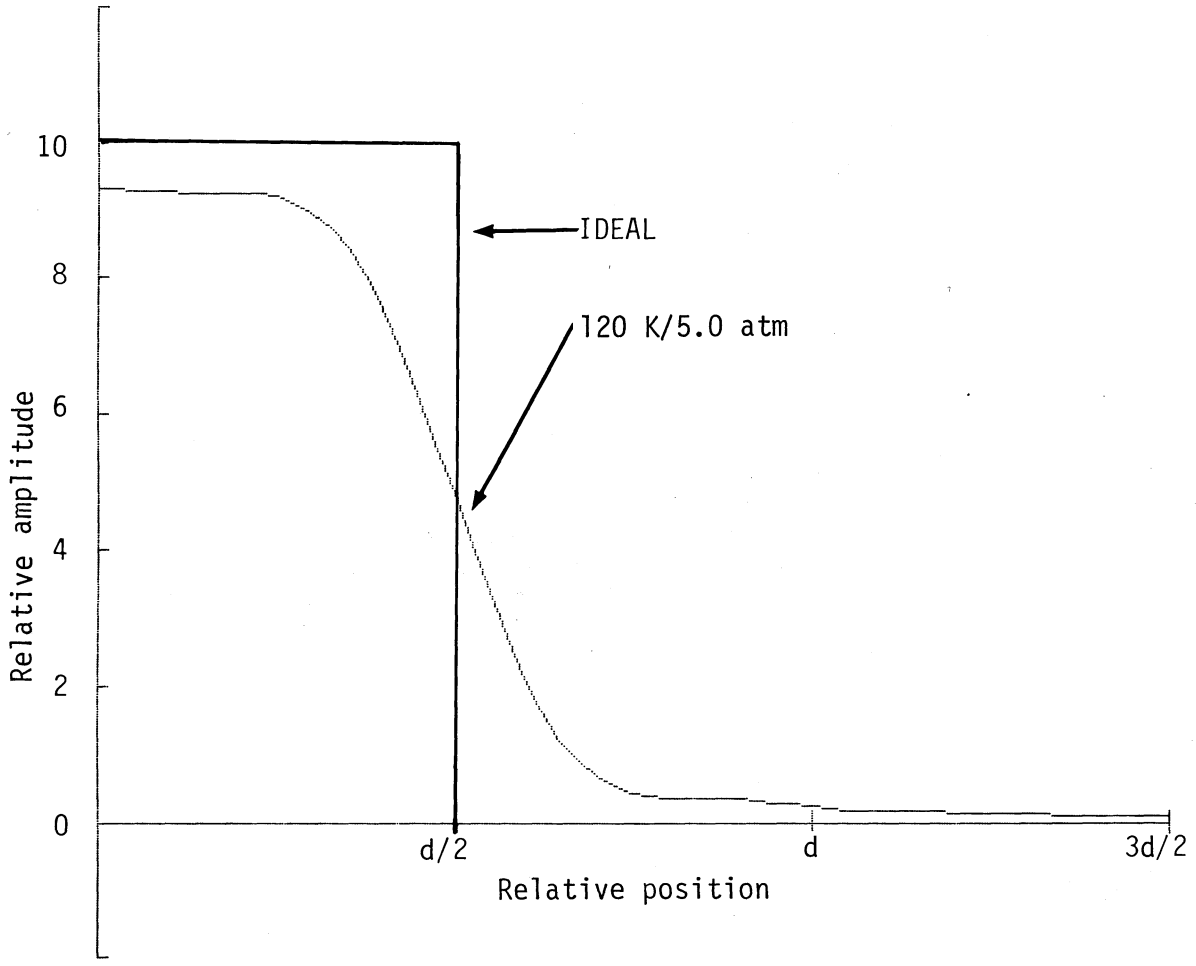

Figure 15.- Effect of square wave response on target contrast.

1. Report No.	2. Government Accession No.	3. Recipient's Catalog No.
NASA TM-84550		

4. Title and Subtitle	5. Report Date
IMAGE DEGRADATION IN LANGLEY 0.3-METER TRANSONIC CRYOGENIC TUNNEL	November 1982
	6. Performing Organization Code: 505-31-63-03
7. Author(s): W. L. Snow, A. W. Burner, and W. K. Goad	8. Performing Organization Report No.: L-15512
	10. Work Unit No.
9. Performing Organization Name and Address: NASA Langley Research Center, Hampton, VA 23665	11. Contract or Grant No.
	13. Type of Report and Period Covered: Technical Memorandum
12. Sponsoring Agency Name and Address: National Aeronautics and Space Administration, Washington, DC 20546	14. Sponsoring Agency Code

15. Supplementary Notes

16. Abstract

The optical quality of gas in a cryogenic wind tunnel was determined by observing Sayce targets through different pathlengths of the medium. The data were used to determine the square wave response of the test gas. At conditions corresponding to 15 times ambient density, considerable decrease in response to higher spatial frequencies was noted even in the absence of flow. Under flow conditions, vibrations further degraded the response. The results are interpreted in terms of possible photogrammetric approaches to measure model deformation in large cryogenic facilities such as the National Transonic Facility.

17. Key Words (Suggested by Author(s))	18. Distribution Statement
National Transonic Facility Langley 0.3-Meter Transonic Cryogenic Tunnel Model deformation Image degradation Square wave response Photogrammetry Optical test targets	Unclassified - Unlimited Subject Category 35

19. Security Classif. (of this report)	20. Security Classif. (of this page)	21. No. of Pages	22. Price
Unclassified	Unclassified	23	A02

For sale by the National Technical Information Service, Springfield, Virginia 22161

NASA-Langley, 1982